Monthly Notices of the ROYAL ASTRONOMICAL SOCIETY

MNRAS **521,** 5013–5025 (2023) https://doi.org/10.1093/mnras/stad849
Advance Access publication 2023 March 22

Beyond – ΛCDM constraints from the full shape clustering measurements from BOSS and eBOSS

Agne Semenaite [1]★ Ariel G. Sánchez [1,2] Andrea Pezzotta,[1] Jiamin Hou,[1,3] Alexander Eggemeier [4] Martin Crocce [5,6] Cheng Zhao,[7] Joel R. Brownstein [8] Graziano Rossi[9] and Donald P. Schneider[10,11]

[1]*Max-Planck-Institut für extraterrestrische Physik, Postfach 1312, Giessenbachstr., D-85748 Garching, Germany*
[2]*Universitäs-Sternwarte Müchen, Scheinerstrasse 1, D-81679 Müchen, Germany*
[3]*Department of Astronomy, University of Florida, 211 Bryant Space Science Center, Gainesville, FL 32611, USA*
[4]*Argelander Fellow, Argelander Institut für Astronomie der Universität Bonn, Auf dem Hügel 71, D-53121 Bonn, Germany*
[5]*Institute of Space Sciences (ICE, CSIC), Campus UAB, Carrer de Can Magrans, s/n, E-08193 Barcelona, Spain*
[6]*Institut d'Estudis Espacials de Catalunya (IEEC), E-08034 Barcelona, Spain*
[7]*Institute of Physics, Laboratory of Astrophysics, École Polytechnique Fédérale de Lausanne (EPFL), Observatoire de Sauverny, CH-1290 Versoix, Switzerland*
[8]*Department of Physics and Astronomy, University of Utah, 115 S. 1400 E., Salt Lake City, UT 84112, USA*
[9]*Department of Physics and Astronomy, Sejong University, Seoul, 143-747, Republic of Korea*
[10]*Department of Astronomy and Astrophysics, The Pennsylvania State University, University Park, PA 16802, USA*
[11]*Institute for Gravitation and the Cosmos, The Pennsylvania State University, University Park, PA 16802, USA*

Accepted 2023 March 16. Received 2023 March 16; in original form 2022 October 13

ABSTRACT

We analyse the full shape of anisotropic clustering measurements from the extended Baryon Oscillation Spectroscopic Survey quasar sample together with the combined galaxy sample from the Baryon Oscillation Spectroscopic Survey. We obtain constraints on the cosmological parameters independent of the Hubble parameter h for the extensions of the Lambda cold dark matter (ΛCDM) models, focusing on cosmologies with free dark energy equation of state parameter w. We combine the clustering constraints with those from the latest cosmic microwave background data from Planck to obtain joint constraints for these cosmologies for w and the additional extension parameters – its time evolution w_a, the physical curvature density ω_K and the neutrino mass sum $\sum m_\nu$. Our joint constraints are consistent with a flat ΛCDM cosmological model within 68 per cent confidence limits. We demonstrate that the Planck data are able to place tight constraints on the clustering amplitude today, σ_{12}, in cosmologies with varying w and present the first constraints for the clustering amplitude for such cosmologies, which is found to be slightly higher than the ΛCDM value. Additionally, we show that when we vary w and allow for non-flat cosmologies and the physical curvature density is used, Planck prefers a curved universe at 4σ significance, which is $\sim 2\sigma$ higher than when using the relative curvature density Ω_K. Finally, when w is varied freely, clustering provides only a modest improvement (of 0.021 eV) on the upper limit of $\sum m_\nu$.

Key words: cosmological parameters – large-scale structure of Universe.

1 INTRODUCTION

The standard cosmological model, Lambda cold dark matter (ΛCDM) predicts a spatially flat Universe, which today is dominated by CDM and dark energy components, the latter believed to be well described by a constant negative equation of state parameter $w = -1$, equivalent to cosmological constant Λ. This model is supported by a number of cosmological observations spanning a range of redshifts, from cosmic microwave background (CMB) power spectra probing the epoch of recombination (Hinshaw et al. 2013; Planck Collaboration VI 2020), to baryonic acoustic oscillation (BAO) feature in galaxy clustering measurements reaching matter-dominated redshifts (Cole et al. 2005; Eisenstein et al. 2005; Anderson et al. 2012; Alam et al. 2017, 2021), to standard candle SN Ia observations that reveal the dominance of dark energy today (Riess et al. 1998; Perlmutter et al. 1999).

Despite this success, the increasingly precise low-redshift measurements have started hinting at discrepancies between the observed ΛCDM parameter values and CMB predictions. Most significantly, the SN measurements of the Hubble parameter (H_0) suggest an expansion rate of the Universe today that is 5σ above the prediction coming from Planck satellite CMB observations (Planck Collaboration VI 2020; Riess et al. 2022). Additionally, there are also inconsistencies surrounding the amplitude of the weak lensing signal, as described by $S_8 = \sigma_8\sqrt{\Omega_m/0.3}$ (where Ω_m is the relative matter density parameter, and σ_8 is the linear density field variance as measured on a scale of 8 h^{-1}Mpc), with different weak lensing surveys finding a value that is 2–3σ below Planck's best-fitting prediction (Heymans et al. 2021; Abbott et al. 2022).

Galaxy clustering has provided the most precise cosmological low-redshift constraints to date (Alam et al. 2021) and is, therefore,

★ E-mail: agne@mpe.mpg.de

crucial in determining whether the discrepancies observed point to a tension between low and high-redshift measurements or are related to specific probes instead. Two-point clustering statistics display two main features that allow us to fit for the background expansion of the Universe and the growth of structure separately. First, the acoustic waves of the baryon-photon plasma in the early pre-recombination Universe appear as the BAO signature – a bump in two-point correlation function, or a series of oscillations in Fourier space, whose physical size is known and can, therefore, be used as a standard ruler to probe the distance–redshift relation. Secondly, each galaxy has a peculiar velocity component due to the coherent motion towards overdense regions, which provides an additional contribution to the measured redshift and results in an anisotropic clustering pattern – the redshift space distortions (RSD). In two-point statistics, this manifests as an angle-dependent change in amplitude, which can be fit to extract cosmology based on the structure growth. Traditionally, the most common approach has been to model and fit the full shape of the clustering measurements (e.g. Percival et al. 2002; Tegmark et al. 2004; Sánchez et al. 2006; Parkinson et al. 2012; Sánchez et al. 2012, 2017). This 'full-shape' analysis has regained attention recently, as it makes use of all of the information available on the statistic being considered (Tröster et al. 2020; d'Amico et al. 2020; Ivanov, Simonović & Zaldarriaga 2020b; Chen, Vlah & White 2021). While some of these analyses did find a lower value of σ_8 (Tröster et al. 2020; Chen et al. 2021), overall, no significant discrepancies with Planck have been reported for clustering constraints alone.

A major issue with the discussion surrounding the consistency between large-scale structure probes and Planck is that it has largely been based on the parameters S_8 and σ_8. Though well measured by weak lensing, the two parameters are defined through h (through the variance scale 8 h^{-1} Mpc for σ_8 and the definition of critical density in Ω_m) and, therefore, depend on the posterior of h recovered by a particular probe. As noted in Sánchez (2020), this approach leads to inconsistencies between different measurements, which make a meaningful comparison non-trivial.

A recent full shape analysis of Baryon Oscillation Spectroscopic Survey (BOSS) galaxy and extended Baryon Oscillation Spectroscopic Survey (eBOSS) quasar (QSO) clustering measurements by Semenaite et al. (2022) has addressed this inconsistency by exploring ΛCDM constraints on the parameter space that is explicitly chosen to not be defined through h. Here, σ_8 is replaced by its equivalent defined on a physical scale of 12 Mpc, σ_{12}, as introduced by Sánchez (2020), and the relative densities Ω are substituted by their physical counterparts $\omega = \Omega h^2$. In this alternative parameter space, the joint clustering data set BOSS + eBOSS shows a near-perfect consistency with the Planck results. Moreover, even when clustering is further combined with weak lensing 3 × 2pt measurements from Dark Energy Survey Year 1 data release (DES Y1; Abbott et al. 2018), the recovered value of σ_{12} is in an excellent agreement with the CMB predicted clustering amplitude.

The tension between weak lensing (and its combination with clustering) and Planck, however, does not disappear completely even in the physical parameter space but is instead reflected in the $\log(10^{10}A_s)-\sigma_{12}$ plane which relates initial (A_s) and final (σ_{12}) amplitudes of density fluctuations. For a given value of σ_{12}, Planck's preferred value of $\log(10^{10}A_s)$ is lower than that of DES or DES + BOSS + eBOSS, indicating a greater predicted amount of structure growth than what is observed by the large-scale structure. Furthermore, when the parameters describing the shape of the power spectrum (spectral index n_s and baryon and cold dark matter densities ω_b and ω_m) are fixed to their Planck best-fitting values, there is also a slight discrepancy in the recovered dark energy density ω_{DE}, with Planck preferring a 1.7σ lower value than DES + BOSS + eBOSS.

While these differences are not yet significant, they are consistent with the amount of tension seen between DES YR1 and Planck (Abbott et al. 2018) and offer a straightforward interpretation within ΛCDM relating differences in structure growth with the poorly constrained ω_{DE}, whose dominance emerges at low-redshift only. As Planck measures CMB at the epoch of recombination ($z_\star$), its predictions for low redshifts, set by the angular diameter distance $D_A(z_\star)$, are extremely sensitive to the model choice. Galaxy clustering, conversely, is directly sensitive to dark energy both through the BAO peak (the line-of-sight measurement allows to constrain the expansion rate H_0 which is just a sum of physical matter and dark energy densities) and the RSD effect (dark energy slowing down the structure growth). Nevertheless, the current clustering constraints on ω_{DE} are at the level of around 6 per cent for a fixed dark energy equation of state parameter $w = -1$, and degrade if w is allowed to vary. None the less, the future Stage IV galaxy surveys, such as the Dark Energy Spectroscopic Instrument (DESI, DESI Collaboration et al. 2016), the ESA space mission *Euclid* (Laureijs et al. 2011), and the Legacy Survey of Space and Time (LSST) at the Rubin Observatory (Ivezić et al. 2019) promise further improved precision on cosmological parameters, including sub-per cent measurements of the fraction of dark energy.

Until these new data become available and in light of the inconsistencies within ΛCDM among the different probes, a number of extensions to the base ΛCDM model may be considered, as has already become standard in many major surveys (Spergel et al. 2003; Campbell et al. 2013; Kitching et al. 2014; Abbott et al. 2019; Planck Collaboration VI 2020; Alam et al. 2021; Tröster et al. 2021; DES Collaboration 2022). While the constraints derived from BAO and RSD summary statistics have mostly focused on combining clustering with CMB or SN data, full shape galaxy clustering analyses have been shown to provide competitive results beyond ΛCDM without requiring combination with any additional probes (Chudaykin, Dolgikh & Ivanov 2021a). Importantly, unlike when using these summary statistics, full shape analyses are not susceptible to the bias due to the h^{-1}Mpc units (RSD effect is usually summarized as a combination of linear growth rate f and σ_8).

With this motivation in mind, this analysis extends the full shape BOSS galaxy and eBOSS QSO clustering analysis of Semenaite et al. (2022) and presents the current physical parameter space constraints for extensions to ΛCDM. In particular, we are interested in models where w is allowed to take values other than $w = -1$, and in the resulting constraints for curvature, neutrino mass, and time-varying equation-of-state parameter in such cosmologies.

Our data and modelling choices remain largely the same as that of Semenaite et al. (2022) (however, we do not explore combinations with weak lensing, but rather make use of SN measurements, as they provide significant additional constraining power at low redshifts, important for evolving dark energy models) and are described in Section 2, which also reviews our physical parameter space and priors used. The results for each of the cosmologies considered are presented in Section 3, together with constraints on selected parameters in Table 2 (additional parameter constraints are presented in the Appendix). We make use of the simplest extension considered, wCDM, to illustrate the advantages of physical parameter space in such extended models and discuss this in Section 3.1. Our conclusions are presented in Section 4.

Table 1. Priors used in our analysis. *U* indicates a flat uniform prior within the specified range, the nuisance parameter priors are listed in the bottom section of the table. Unless stated otherwise, the priors on the cosmological and clustering nuisance parameters match those of Semenaite et al. (2022).

Parameter	Prior
$\Omega_b h^2$	$U(0.019, 0.026)$
$\Omega_c h^2$	$U(0.01, 0.2)$
$100\theta_{MC}$	$U(0.5, 10.0)$
τ	$U(0.01, 0.8)$
$\ln(10^{10}A_s)$	$U(1.5, 4.0)$
n_s	$U(0.5, 1.5)$
w	$U(-3 - 0.3)$
w_a	$U(-2, 2)$
Ω_K	$U(-0.3, 0.3)$
$\sum m_\nu$	$U(0.0, 2.0)$
b_1	$U(0.5, 9.0)$
b_2	$U(-4, 8.0)$
a_{vir}	$U(0.0, 12.0)$
σ_{err} (eBOSS only)	$U(0.01, 6.0)$

2 METHODOLOGY

This analysis is a follow-up on the work by Semenaite et al. (2022) and uses the same clustering measurements and modelling choices. In this section, we, therefore, only provide a summary of the main points, referring the reader to Semenaite et al. (2022) and the references therein for a more detailed description.

2.1 Galaxy and QSO clustering measurements

We consider configuration space clustering measurements from BOSS galaxy samples (Dawson et al. 2013) and eBOSS QSO catalogue (Dawson et al. 2016; Lyke et al. 2020), which are part of Sloan Digital Survey Data Release 12 (SDSS DR12; Alam et al. 2015; Reid et al. 2016) and Data Release 16 (SDSS DR16; Ahumada et al. 2020; Ross et al. 2020), respectively. Each of the two data vectors represent a measurement of the anisotropic two point correlation function $\xi(s, \mu)$, where s is the comoving galaxy separation and μ is the cosine of the angle between the separation vector and the line of sight, compressed into either clustering wedges (for BOSS galaxies) or Legendre multipoles (eBOSS QSO). The two statistics carry equivalent information and clustering wedges may be expressed as a linear combination of multipoles. Following the fiducial analyses, for all clustering data North Galactic Cap and South Galactic Cap measurements are analysed together.

We consider BOSS galaxy clustering wedges measurements from Sánchez et al. (2017) based on the combined galaxy sample (Reid et al. 2016) in two redshift bins: $0.2 < z < 0.5$ (corresponding to an effective redshift $z_{eff} = 0.38$) and $0.5 < z < 0.75$ ($z_{eff} = 0.61$). The clustering wedges statistic (Kazin, Sánchez & Blanton 2012) is defined as the average of $\xi(s, \mu)$ over an angular interval $\Delta\mu = \mu_2 - \mu_1$. Here, the clustering wedges are measured in three equal width intervals covering μ range 0 to 1. The covariance matrices for these data are estimated from the set of 2045 MD-PATCHY mock catalogues (Kitaura et al. 2016).

For the clustering of eBOSS QSO sample, we use Legendre multipole measurements of Hou et al. (2021). Here, $\xi(s, \mu)$ is expressed in Legendre polynomial basis and we consider the non-vanishing multipoles $\ell = 0, 2, 4$. The QSO sample covers the redshift range of $0.8 < z < 2.2$, with $z_{eff} = 1.48$ and the covariance matrix is obtained using a set of 1000 mock catalogues, as described in Zhao et al. (2021).

The treatment of BOSS and eBOSS QSO clustering measurements matches the original treatment by Sánchez et al. (2017) and Hou et al. (2021): we consider the scales of $20\,h^{-1}$Mpc $< s < 160\,h^{-1}$Mpc and assume a Gaussian likelihood for each set of measurements, which are taken to be independent (as they do not overlap in redshift). The covariances are kept fixed and we account for the finite number of mock catalogues used in their derivation (Kaufman 1967; Hartlap, Simon & Schneider 2007; Percival et al. 2014).

2.2 Model

The model for the full shape galaxy clustering wedges and Legendre multipoles used in this analysis is identical to that of Semenaite et al. (2022): we use a response function based approach for the non-linear matter power spectrum predictions (as in the original eBOSS QSO analysis by Hou et al. 2021). We model galaxy bias at one loop and make use of co-evolution relations for the tidal bias parameters (motivated by the findings of Eggemeier et al. 2021) and account for RSD and Alcock–Paczynski (AP) distortions (Alcock & Paczyński 1979) as described in the original wedges analysis in Sánchez et al. (2017). We also correct for the non-negligible redshift errors in the QSO sample (Zarrouk et al. 2018) following Hou et al. (2018) and including a damping factor to the power spectrum, $\exp(-k\mu\sigma_{err})$, with σ_{err} as a free parameter.

Our model predictions for the non-linear matter power spectrum $P_{mm}(k)$ (the Fourier space equivalent of $\xi(s)$) are obtained using the Rapid and Efficient SPectrum calculation based on RESponSe functiOn approach (RESPRESSO; Nishimichi, Bernardeau & Taruya 2017). The key ingredient here is the response function, which quantifies the variation of the non-linear matter power spectrum at scale k induced by a change in linear power spectrum at scale q. Given a fiducial measurement of $P_{mm}(k|\boldsymbol{\theta}_{fid})$ from a set of N-body simulations with cosmological parameters $\boldsymbol{\theta}_{fid}$, the response function allows one to obtain a prediction for $P_{mm}(k)$ for an arbitrary cosmology with multistep reconstruction used for cosmologies that differ considerably from the fiducial one. In RESPRESSO, $\boldsymbol{\theta}_{fid}$ corresponds to the best-fitting ΛCDM model to the Planck 2015 data (Planck Collaboration XIII 2016). The response function is modelled using the phenomenological model of Nishimichi, Bernardeau & Taruya (2016) based on renormalized perturbation theory (Taruya et al. 2012).

Our bias model follows Eggemeier, Scoccimarro & Smith (2019) and relates the matter density fluctuations δ_m to the galaxy density fluctuations δ at one loop:

$$\delta = b_1\delta_m + \frac{b_2}{2}\delta_m^2 + \gamma_2\mathcal{G}_2(\Phi_v) + \gamma_{21}\mathcal{G}_2(\varphi_1, \varphi_2) + ... \quad (1)$$

Here, the Galileon operators $\mathcal{G}_2$ of the normalized velocity potential Φ_v and linear and second-order Lagrangian perturbation potentials φ_1 and φ_2 are defined as

$$\mathcal{G}_2(\Phi_v) = (\nabla_{ij}\Phi_v)^2 - (\nabla^2\Phi_v)^2, \quad (2)$$

$$\mathcal{G}_2(\varphi_1, \varphi_2) = \nabla_{ij}\varphi_2\nabla_{ij}\varphi_1 - \nabla^2\varphi_2\nabla^2\varphi_1. \quad (3)$$

In order to reduce the number of free parameters, we express the tidal bias parameters γ_2 and γ_{21} in terms of linear bias b_1, as

$$\gamma_2 = 0.524 - 0.547b_1 + 0.046b_1^2, \quad (4)$$

$$\gamma_{21} = -\tfrac{2}{21}(b_1 - 1) + \tfrac{6}{7}\gamma_2. \quad (5)$$

Here, the relation for γ_2 is as obtained by Sheth, Chan & Scoccimarro (2013) using excursion set theory, while γ_{21} is set by assuming

Table 2. Marginalized posterior constraints (mean values with 68 per cent confidence interval, for $\sum m_\nu$ – 95 per cent confidence interval) derived from Planck CMB and the full shape analysis of BOSS + eBOSS clustering measurements on their own, as well as in combination with each other and with Pantheon SN Ia measurements. All of the models considered here vary the dark energy equation of state parameter w. In addition to this, w_aCDM also varies w_a, allowing for the equation of state parameter that evolves with redshift, w*K*CDM varies curvature, and $w\nu$CDM varies neutrino mass sum $\sum m_\nu$. Note that for w*K*CDM the joint BOSS + eBOSS + Planck constraints should be interpreted bearing in mind that BOSS + eBOSS and Planck are discrepant in this parameter space (Fig. 4). Further constraints, including those on parameters defined through h (relative densities, σ_8), are available in the Appendix.

		Planck	BOSS + eBOSS	BOSS + eBOSS + Planck	BOSS + eBOSS + Planck + SN
wCDM	σ_{12}	0.816 ± 0.011	$0.775^{+0.055}_{-0.066}$	0.804 ± 0.010	0.8023 ± 0.0097
	$\omega_{\rm DE}$	$0.509^{+0.15}_{-0.054}$	$0.352^{+0.033}_{-0.044}$	$0.341^{+0.020}_{-0.023}$	0.329 ± 0.012
	w	$-1.41^{+0.11}_{-0.27}$	-1.10 ± 0.13	$-1.066^{+0.057}_{-0.052}$	-1.033 ± 0.031
w_aCDM	σ_{12}	0.816 ± 0.012	$0.768^{+0.053}_{-0.061}$	0.807 ± 0.011	0.805 ± 0.010
	$\omega_{\rm DE}$	$0.494^{+0.17}_{-0.062}$	$0.356^{+0.042}_{-0.059}$	$0.322^{+0.026}_{-0.039}$	0.330 ± 0.012
	w_0	$-1.22^{+0.33}_{-0.39}$	-1.09 ± 0.30	$-0.87^{+0.27}_{-0.22}$	-0.955 ± 0.086
	w_a	<-0.330	$-0.13^{+1.1}_{-0.94}$	-0.60 ± 0.68	$-0.34^{+0.36}_{-0.30}$
w*K*CDM	σ_{12}	0.896 ± 0.029	$0.754^{+0.056}_{-0.062}$	0.809 ± 0.011	0.804 ± 0.010
	$\omega_{\rm DE}$	$0.323^{+0.073}_{-0.20}$	$0.394^{+0.046}_{-0.053}$	$0.346^{+0.020}_{-0.024}$	0.327 ± 0.012
	w	$-1.57^{+0.67}_{-0.38}$	$-0.921^{+0.15}_{-0.093}$	$-1.108^{+0.078}_{-0.067}$	-1.044 ± 0.036
	ω_K	$-0.0116^{+0.0029}_{-0.0036}$	-0.057 ± 0.037	-0.0012 ± 0.0013	-0.0006 ± 0.0011
$w\nu$CDM	σ_{12}	$0.810^{+0.019}_{-0.012}$	$0.767^{+0.053}_{-0.064}$	$0.796^{+0.016}_{-0.012}$	$0.799^{+0.014}_{-0.011}$
	$\omega_{\rm DE}$	$0.508^{+0.15}_{-0.061}$	$0.353^{+0.036}_{-0.046}$	$0.346^{+0.020}_{-0.025}$	0.329 ± 0.012
	w	$-1.43^{+0.16}_{-0.26}$	$-1.16^{+0.16}_{-0.13}$	$-1.102^{+0.086}_{-0.058}$	$-1.040^{+0.038}_{-0.033}$
	$\sum m_\nu$ (eV)	<0.321	<1.34	<0.300	<0.211

conserved evolution of tracers after their formation (Fry 1996; Catelan et al. 1998; Catelan, Porciani & Kamionkowski 2000; Chan, Scoccimarro & Sheth 2012). Using these relations the only free parameters in the bias model are linear and quadratic bias parameters b_1 and b_2. Pezzotta et al. (2021) tested these relations together with non-linear matter power spectrum prescription from RESPRESSO and demonstrated that for BOSS-like samples this approach returns unbiased cosmological constraints.

Our RSD description follows Scoccimarro (2004) and Taruya, Nishimichi & Saito (2010) with the two-dimensional redshift-space power spectrum written as a product of the 'no-virial' power spectrum, $P_{\rm novir}(k, \mu)$, and a non-linear correction due to fingers of God or galaxy virial motions $W_\infty(\lambda = ifk\mu)$:

$$P(k, \mu) = W_\infty(ifk\mu)\, P_{\rm novir}(k, \mu). \tag{6}$$

$P_{\rm novir}(k, \mu)$ is computed using a one-loop approximation that consists of a term that corresponds to the non-linear version of the Kaiser formula (Kaiser 1987) and two higher order terms which account for cross- and bispectrum contributions from density and velocity fields. The corresponding velocity–velocity and matter-velocity power spectra are obtained from empirical relations measured from N-body simulations (Bel et al. 2019). Finally, the virial correction W_∞ is parametrized as (Sánchez et al. 2017):

$$W_\infty(\lambda) = \frac{1}{\sqrt{1 - \lambda^2 a_{\rm vir}^2}} \exp\left(\frac{\lambda^2 \sigma_v^2}{1 - \lambda^2 a_{\rm vir}^2}\right). \tag{7}$$

W_∞ is characterized by a single free parameter $a_{\rm vir}$ which describes the kurtosis of the small-scale velocity distribution. The one-dimensional linear velocity dispersion $\sigma_{\rm v}$ is defined in terms of the linear matter power spectrum $P_{\rm L}$:

$$\sigma_v^2 \equiv \frac{1}{6\pi^2} \int {\rm d}k\, P_{\rm L}(k). \tag{8}$$

We account for AP distortions due to the difference between true and fiducial cosmologies by introducing the geometric distortion factors. The line-of-sight distortion ($q_\parallel$) is characterized by the ratio of Hubble parameters evaluated at the effective redshift in the fiducial ($H'(z_{\rm eff})$) and true ($H(z_{\rm eff})$) cosmologies. Equivalently, the distortions perpendicular to the line of sight ($q_\perp$) are described by the ratio of comoving angular diameter distances $D_{\rm M}(z)$:

$$q_\perp = D_{\rm M}(z_{\rm eff})/D'_{\rm M}(z_{\rm eff}), \tag{9}$$

$$q_\parallel = H'(z_{\rm eff})/H(z_{\rm eff}). \tag{10}$$

The distortion factors are then used to rescale angles μ and galaxy separations s such that

$$s = s' \left(q_\parallel^2 \mu'^2 + q_\perp^2 (1 - \mu'^2)\right), \tag{11}$$

$$\mu = \mu' \frac{q_\parallel}{\sqrt{q_\parallel^2 \mu'^2 + q_\perp^2 (1 - \mu'^2)}}. \tag{12}$$

Our model, therefore, has a total of four free parameters (three for BOSS): b_1, b_2, $a_{\rm vir}$, and $\sigma_{\rm err}$. For more details and model validation, see Semenaite et al. (2022). While our model was tested on mocks that correspond to ΛCDM cosmologies, we expect the results of these tests to be applicable to the extended models as well. The cosmology extensions that we consider (with the exception of massive neutrinos) have the effect of additionally rescaling the amplitude of the matter power spectrum with the final result equivalent to a power spectrum of a ΛCDM cosmology with an adjusted amplitude, σ_{12}, as discussed in Sánchez et al. (2022).

2.3 Additional data

We explore the consistency of our clustering data with the CMB temperature and polarization power spectra from *Planck* satellite

(Planck Collaboration VI 2020). We use public nuisance parameter-marginalized likelihood `plik_lite_TTTEEE+lowl + lowE` and do not include CMB lensing information. In addition to these constraints, we also supplement clustering information with that from SNe Ia from the combined 'Pantheon' sample (Scolnic et al. 2018), consisting of measurements from 1048 SNe Ia in the redshift range of $0.01 < z < 2.3$. We obtain SN cosmological constraints from the JLA likelihood module as implemented in CosmoMC (Lewis & Bridle 2002).

2.4 Parameters and priors

As in Semenaite et al. (2022), we are interested in constraining the cosmological parameters that are defined through physical units (i.e. avoiding h), as many standard cosmological parameter definitions imply averaging over the recovered posterior of h (for a more in-depth discussion see Sánchez 2020; Semenaite et al. 2022). This means that first, instead of describing the clustering amplitude today via σ_8, we use its equivalent defined on the physical scale of 12 Mpc, σ_{12}, as suggested by Sánchez (2020), and second, we use physical (ω_i) rather the fractional (Ω_i) densities of different components i of the energy budget of the Universe with the two quantities related through:

$$\Omega_i = \omega_i / h^2. \tag{13}$$

When considering extended cosmologies, we expect our chosen parameter space to be most relevant for the cases where the ΛCDM assumptions about dark energy are relaxed, as physical dark energy density $\omega_{\rm DE}$ is not well constrained by the CMB or large-scale structure probes and depends on the assumed dark energy model. This statement is especially true for Planck, which probes the Universe at the redshift of recombination. The dimensionless Hubble parameter, h, is defined by the sum of all energy contributions from baryons ($\omega_{\rm b}$), cold dark matter ($\omega_{\rm c}$), neutrinos (ω_ν), dark energy, and curvature (ω_K):

$$h^2 = \omega_{\rm b} + \omega_{\rm c} + \omega_\nu + \omega_{\rm DE} + \omega_K, \tag{14}$$

with dark energy comprising the majority of the total energy budget today. Therefore, when we introduce additional freedom to dark energy modelling, this is also reflected in the constraints on h and any parameter that is defined through it. In this analysis we, therefore, allow the dark energy equation of state parameter $w = p_{\rm DE}/\rho_{\rm DE}$ deviate from its ΛCDM value of $w = -1$ and treat it as a free parameter for all extensions considered in order to explore the effects on physical parameter space constraints.[1]

In addition to the basic wCDM model with constant w, we also consider a more general parametrization where w is allowed to evolve with the scale factor a (Chevallier & Polarski 2001; Linder 2003):

$$w = w_0 + w_a(1 - a). \tag{15}$$

Here, w_0 and w_a are free parameters; we refer to this case as w_aCDM model. We also explore wKCDM – non-flat models with $\Omega_k \neq 0$. Here, as with the other energy budget components, we are interested in physical curvature density $\omega_k = \Omega_k h^2$. Finally, we investigate the constraints on neutrino mass sum $\sum m_\nu$, by allowing it to vary freely instead of fixing it to the fiducial value of $\sum m_\nu = 0.06$eV, corresponding to the minimum value allowed by neutrino oscillation experiments under normal hierarchy (Otten & Weinheimer 2008). We refer to this model as $w\nu$CDM.

We use CosmoMC (Lewis & Bridle 2002) to perform Monte chain Markov Carlo (MCMC) sampling. For the linear-theory matter power spectrum prediction, CosmoMC uses CAMB (Lewis, Challinor & Lasenby 2000), adapted to compute the theoretical model for anisotropic clustering measurements, as described in Section 2.2. In addition to the nuisance parameters, listed in Table 1, we sample over the basis cosmological parameters used by CosmoMC:

$$\boldsymbol{\theta}_{\rm base} = \left(\omega_{\rm b}, \omega_{\rm c}, \Theta_{\rm MC}, A_{\rm s}, n_{\rm s}, w_0, w_a, \Omega_k, \sum m_\nu\right), \tag{16}$$

where $\Theta_{\rm MC}$ is 100 times the approximate angular size of the sound horizon at recombination. For each of the models described in this section we only vary the relevant extended parameters, fixing the rest to their fiducial values, as described above. We impose flat and uninformative priors, except for $\omega_{\rm b}$, with the priors for ΛCDM parameters matching those of Semenaite et al. (2022). Our flat prior for $\omega_{\rm b}$ informs clustering measurements, as they do not constrain this parameter on their own, and is 25 times wider than the corresponding Planck constraint. We also need to specify the allowed values of the Hubble parameter, h. In order to be consistent with Semenaite et al. (2022), we choose the same range of $0.5 < h < 0.9$. While this range is somewhat restrictive for Planck on its own for varying dark energy cosmologies, these limits have little effect on the physical parameter space that we consider, and are mostly uninformative once Planck is combined with clustering or when considering clustering alone. Finally, these limits are motivated by the direct measurements of H_0, which fall well within this range (Reid et al. 2013; Birrer et al. 2020; Kourkchi et al. 2020; Riess et al. 2022; Hagstotz, Reischke & Lilow 2022). A summary of all cosmological priors used in this analysis is presented in Table 1.

3 RESULTS

We are mainly interested in clustering constraints from BOSS + eBOSS as well as their combination with Planck. Where found informative, we supplement the clustering constraints with those from SNe Ia. The summary of our results on the main parameters of interest is shown in Table 2 with further constraints available in Appendix A. We present our parameter constraints in terms of marginalized posterior mean values with corresponding 68 per cent confidence intervals (95 per cent for $\sum m_\nu$). As we perform MCMC sampling to obtain our constraints, we only have a noisy estimate of the true best-fitting values, which, however, are all within an order of a standard deviation from the corresponding means. Because of this, and due to the fact that we find our likelihood surface to be fairly flat, with all fits within 1σ of mean cosmological parameter values providing excellent fits, we choose to not present the best-fitting values among our results.

3.1 Evolving dark energy – wCDM

ΛCDM assumes a cosmological constant-like behaviour for dark energy with a fixed $w = -1$. Nevertheless, w may be allowed to deviate from this value and be treated as a free parameter. As the simplest of the models considered here, we will use our results for wCDM to illustrate the behaviour of our data in the physical parameter space for this class of cosmologies. Fig. 1 presents our constraints from BOSS + eBOSS and Planck on their own (light and dark blue, respectively) as well as their combination (in red)

[1] While our wide uninformative w prior is in line with the commonly adopted range, it may be noted that extremely negative values for this parameter violate the Null Energy Condition, as noted in, for example, Colgáin & Sheikh-Jabbari (2021).

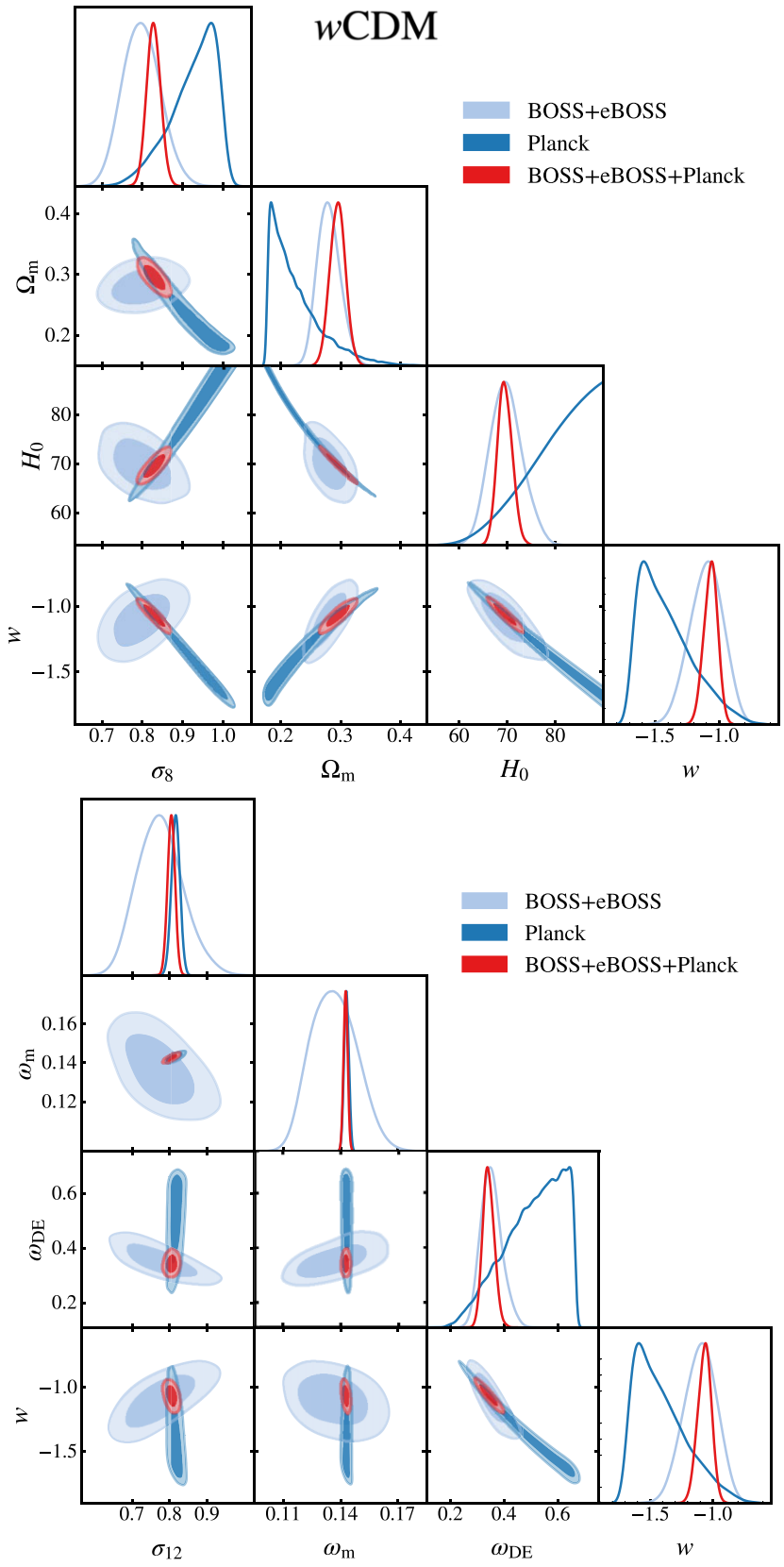

Figure 1. Marginalized posterior contours in the 'traditional' and h-independent parameter spaces derived from the full shape of anisotropic clustering measurements of BOSS DR12 galaxies in combination with eBOSS QSOs (light blue) and CMB measurements by Planck (dark blue) for a wCDM model. The joint constraints are shown in red. In physical parameter space, Planck is able to constrain the clustering amplitude today σ_{12} even in models with free w.

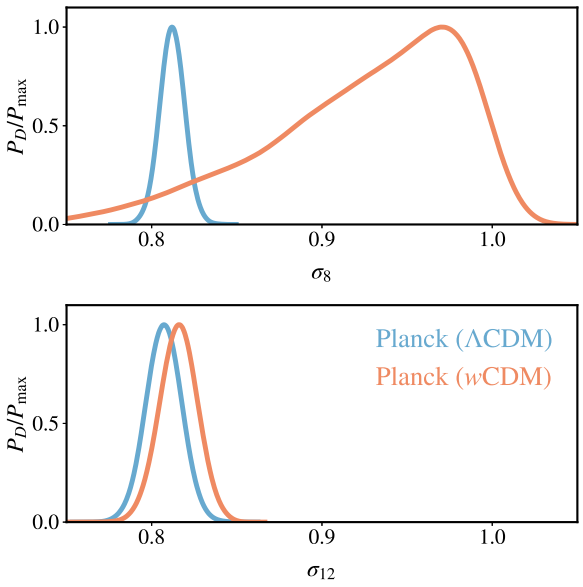

Figure 2. Upper panel: One-dimensional marginalized Planck posteriors for σ_8 for ΛCDM (blue) and wCDM (orange) cosmologies. Lower panel: The corresponding posteriors of σ_{12}. The difference between two panels is due to h^{-1}Mpc units used to define the scale at which the linear density field variance is measured for σ_8. As Planck does not constrain H_0 well once w is allowed to freely vary, the resulting posterior, over which the clustering amplitude is effectively averaged, is extremely wide and results in degraded constraint on σ_8. The parameter σ_{12} is not affected by this issue, as it is defined on a Mpc scale – the precision of the measurement for Planck is the same in both cosmologies shown.

with constraints on the standard parameter space shown in the upper panel for comparison.

Comparing the two sets of panels in Fig. 1, it is clear that the posterior degeneracy directions for H_0 (whose value is determined by the sum of the physical densities of all the components) are set by the $\omega_{\rm DE}$ component. For Planck, the constraint on $\omega_{\rm DE}$ is set by the prior – as discussed before, Planck does not probe the redshifts at which dark energy becomes dominant directly, but rather is able to provide model-dependent constraints based on $D_{\rm A}(z_\star)$. The CMB observations, therefore, do not constrain dark energy density once the evolution of this component is not well defined.

In contrast, $\omega_{\rm m}$ is set by the scale dependence on the amplitude of CMB spectra (for a fixed acoustic angular scale) and is not sensitive to the assumptions on dark energy. Following H_0, any parameter defined through it also exhibits similar degeneracies, as they are effectively averaged over the posterior of H_0 – as a result, σ_8 and $\Omega_{\rm m}$ are not well constrained by Planck either.

None the less, importantly, that does not mean that Planck is unable to measure the clustering amplitude today – the wCDM constraint on σ_{12} has the same precision as in ΛCDM model, as illustrated in Fig. 2. The lack in constraining power on σ_8 is, therefore, an artefact of using h^{-1}Mpc units. To understand why Planck does not lose constraining power on σ_{12} even in extended cosmologies, one can first note that w and σ_{12} show almost no correlation for this probe. This behaviour arises because the change in w is compensated by a change in $\omega_{\rm DE}$, as is evident from Planck's constraints in the $w - \omega_{\rm DE}$ plane: only certain combinations of these parameters, set by $D_{\rm A}(z_\star)$, are allowed, with the resulting degeneracy corresponding to a constant σ_{12}. This result means that a preference for more negative w closely corresponds to an increase in $\omega_{\rm DE}$.

Our analysis is, therefore, the first one to quote a CMB constraint on clustering amplitude today in cosmologies with varying w. The Planck best-fitting value of $\sigma_{12} = 0.816 \pm 0.011$ that we find for wCDM model is slightly higher than that for ΛCDM (0.807 ± 0.011) – this increase is because the higher values of $\omega_{\rm DE}$ allowed in wCDM correspond to a more negative w, thus the dark energy content is lower at the start of the epoch when this component becomes relevant, which results in slightly more total structure growth. Nevertheless, as σ_{12} is mostly determined by the physical matter density, as discussed above, this shift in the clustering amplitude value is minimal.

The advantage of our physical parameter space is most evident for Planck due to its lack of constraining power on H_0; none the less, even for clustering probes, the precision on physical parameter constraints degrades less, compared to their h-dependent counterparts, once dark energy model assumptions are relaxed.

While clustering on its own prefers a mean equation of state parameter value that is compatible with $w = -1$ ($w = -1.10 \pm 0.13$), for Planck and the combination BOSS + eBOSS + Planck, the fiducial value is just outside of the 68 per cent confidence limit. This result appears because of the significant volume of Planck's posterior corresponding to models with high dark energy content, which shifts the mean w. The addition of low redshift information from clustering rules out such models and brings the joint constraints closer to ΛCDM.

Comparing our BOSS + eBOSS + Planck constraints with previously published full shape analysis of BOSS clustering wedges by Sánchez et al. (2017), who obtain $w = -0.991^{+0.062}_{-0.047}$ for BOSS + Planck (2015), reveals that our updated analysis shifts the mean w by $\sim 1\sigma$ towards more negative values. This result may be attributable to a number of differences between the analyses, most notably the updated CMB measurements from Planck.

In addition to this approach, Brieden, Gil-Marín & Verde (2022) performed a reconstructed power spectrum multipole analysis of BOSS DR12 LRG and eBOSS QSO samples. In this analysis, the information from BAO and RSD summary statistics is complemented by additional summary statistic derived from the shape of the power spectrum (ShapeFit, Brieden, Gil-Marín & Verde 2021). Our BOSS + eBOSS (+Planck) constraint $w = -1.10 \pm 0.13$ ($w = -1.066^{+0.057}_{-0.052}$) agrees well with that of Brieden et al. (2022): $w = -0.998^{+0.085}_{-0.073}$ ($w = -1.093^{+0.048}_{-0.044}$), showing the robustness of these results.

3.2 Evolving dark energy equation of state – w_aCDM

We further generalize the dark energy description allowing its equation of state parameter to vary with time, as defined in equation (15). Fig. 3 shows our constraints for the dark energy parameters: w, $w_{\rm a}$, $\omega_{\rm DE}$. Here, we combine our clustering constraints with SNe Ia, which provide background constraints for the lowest redshifts and are, therefore, extremely useful for probing the evolution of dark energy.

The additional freedom in the equation of state model has minimal impact on the constraints on σ_{12} and $\omega_{\rm DE}$. However, the addition of SN Ia data halves the error on dark energy density with the resulting constraint of $\omega_{\rm DE} = 0.330 \pm 0.012$. All of the data set combinations considered recover a value of w_0 that is consistent with -1, although with significantly larger uncertainty than in wCDM. Planck does not constrain $w_{\rm a}$ on its own, but combining it with the clustering and SN data yields a value compatible with no evolution (for BOSS + eBOSS + Planck + SN $w_a = -0.34^{+0.36}_{-0.30}$).

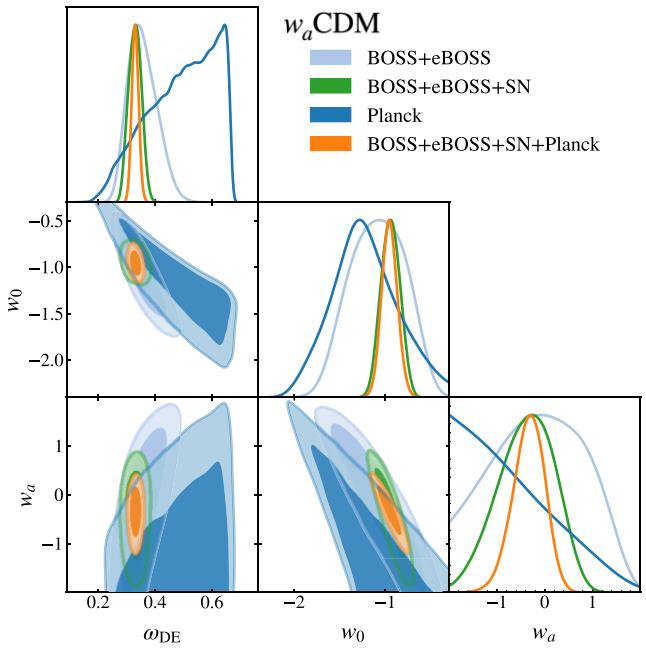

Figure 3. Marginalized posterior contours for dark energy parameters in *wa*CDM, where the dark energy equation-of-state parameter w is allowed to evolve in time, as defined in equation (15). We show constraints from the full-shape clustering analysis of BOSS DR12 galaxies in combination with eBOSS QSOs (light blue), their combination with Pantheon SN Ia measurements (green), CMB constraints by Planck (in dark blue), and the combination of all four data sets (in orange).

We may compare our constraints with those from the completed SDSS consensus analysis by Alam et al. (2021), although note that they use additional data sets, including eBOSS luminous red galaxy and emission line galaxy samples as well as BAO from the Ly α forest, and use summary statistics for BAO and RSD to obtain the joint constraints. The consensus analysis also uses reconstructed BAO, while we perform no reconstruction in this work. The quoted constraints for combined Planck + Pantheon SNe, SDSS BAO + RSD and DES 3 $\times$ 2pt data are $w_0 = -0.939 \pm 0.073$ and $w_a = -0.31^{+0.28}_{-0.24}$, which are in excellent agreement with our BOSS + eBOSS + Planck + SN result.

Chudaykin, Dolgikh & Ivanov (2021b) also performed a full shape analysis using a model based on the Effective Field Theory of Large Scale Structure (EFT; Baumann et al. 2012). They analysed BOSS DR12 luminous red galaxy redshift space power spectrum multipoles in combination with BAO measurements from post-reconstructed power spectra of BOSS DR12 supplemented with a number of additional BAO measurements from SDSS, including those from eBOSS QSO sample and additionally augmented by adding SN Ia measurements from Pantheon (as also done in this work). Their final constraints of $w_0 = -0.98^{+0.10}_{-0.11}$ and $w_a = -0.32^{+0.63}_{-0.48}$ are tighter than ours (most likely due to the additional BAO data) but in an excellent agreement with our BOSS + eBOSS + SN results: $w_0 = -0.94^{+0.20}_{-0.19}$ and $w_a = -0.40^{+1.0}_{-1.2}$. It is additionally important to note that EFT-based constraints have been shown to depend on the counterterm prior choices (Simon et al. 2022; Carrilho, Moretti & Pourtsidou 2023).

3.3 Non-zero curvature – *wK*CDM

We explore what occurs when, in addition to varying w (but with $w_a = 0$), we also allow for non-flat models. The resulting constraints are shown in Fig. 4. Here, together with the dark energy parameter constraints, we also display the physical curvature density $\omega_K = \Omega_K h^2$.

It is interesting that the Planck data constrain the physical curvature well, with the mean value of $\omega_K = -0.0116^{+0.0029}_{-0.0036}$, indicating a strong preference for non-zero curvature. We compare this result with the constraint on the h-dependent equivalent, $\Omega_K = -0.030^{+0.018}_{-0.010}$, note how physical units allow us to detect the deviation from flatness at a higher significance (4σ for ω_K versus 1.6σ for Ω_K). This preference for closed Universe is a known feature of Planck data and believed to be related to the lensing anomaly (Planck Collaboration VI 2020). None the less, our physical curvature constraint indicates the most significant deviation from flat Universe yet, which is especially interesting bearing in mind that, in addition to curvature, we are also varying w and would, therefore, expect a somewhat more significant preference for closed Universe in fixed $w = -1$ case (however, as seen in Fig. 4, dark energy parameters are almost independent of ω_K for Planck; therefore, we expect the change in the result to be minimal).

Recently, Glanville, Howlett & Davis (2022) reported that clustering data alone may show a 2σ preference for a closed universe. There, a full shape analysis based on EFT is performed on the power spectra multipoles from the full combined 6dFGS, BOSS, and eBOSS catalogues. The analysis by Chudaykin et al. (2021b), however, finds a less significant deviation of $\sim 1\sigma$. Neither of these analyses vary w, which allows for somewhat tighter constraints than what we expect for *wK*CDM (as seen in Fig. 4, clustering exhibits some degeneracy between the two parameters). The mean value of ω_K preferred by BOSS + eBOSS in our analysis, $\omega_K = -0.057 \pm 0.037$, also deviates from 0, but is consistent with flatness at 95 per cent confidence level, indicating no significant preference for a closed universe. In terms of dark energy constraints, the effect of allowing a free varied curvature for clustering is to allow for larger values of ω_{DE}.

CMB and clustering data sets are highly complementary in *wK*CDM, with Planck providing a measurement on curvature and BOSS + eBOSS constraining dark energy parameters. Nevertheless, the two data sets are discrepant within this cosmology. This behaviour is most clear from the $w - \omega_{DE}$ projection in which the 2σ regions of the two sets of contours show little overlap. As discussed before, this particular degeneracy is defined by the clustering amplitude today, so this discrepancy is also reflected in the σ_{12} constraints, with Planck preferring a 2.4σ higher value. This model displays the greatest shift in Planck's σ_{12} out of all of the cosmologies considered in this work.

A discrepancy between Planck and BAO measurements and Planck and full shape analysis of clustering measurements was also found in previous work that varied curvature but kept w fixed (Di Valentino, Melchiorri & Silk 2020; Handley 2021; Vagnozzi et al. 2021; Glanville et al. 2022). Our analysis, therefore, demonstrates that degradation of constraining power when varying w does not provide a solution to this tension (although see also Bel et al. 2022, for 'clustering ratio' based analysis which shows agreement between clustering and CMB even in curved models).

Planck's lensing anomaly, which is related to the preference for non-zero curvature, can be characterized by the phenomenological parameter A_{lens}, which scales the amplitude of the lensing power relative to the physical value. In the absence of systematics or non-standard physics, $A_{lens} = 1$ and is highly degenerate with the measured cosmological parameters that set the amplitude of the power spectrum at late times – σ_{12} and ω_K. Fig. 5, illustrates how allowing A_{lens} to freely vary extends Planck's posterior contours to include $\omega_K = 0$ within 2σ and, therefore, recovers flat ΛCDM. The extension

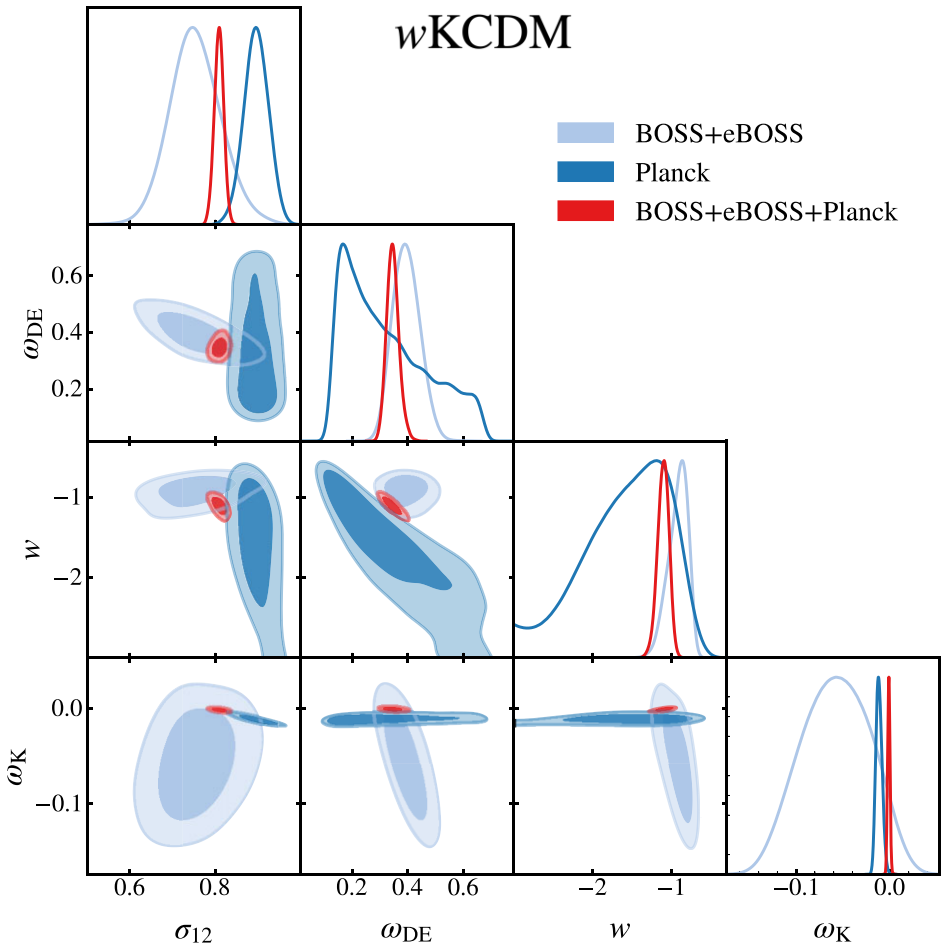

Figure 4. Marginalized posterior contours for dark energy parameters and physical matter and curvature densities in *w*KCDM, where, in addition to varying w, we also allow for non-zero curvature. The constraints from the full-shape clustering analysis of BOSS DR12 galaxies in combination with eBOSS QSOs are shown in light blue, CMB constraints by Planck are displayed in dark blue and the combination of the two sets of probes is shown in red. Note the discrepancy between Planck and BOSS + eBOSS in σ_{12} as well as w–ω_{DE} plane.

of Planck's posterior distribution of σ_{12} to lower values allows for a reconciliation with the constraints from BOSS + eBOSS and reduces the mean σ_{12} inferred from the combined BOSS + eBOSS + Planck analysis. Varying A_{lens} allows to compensate for the excess lensing and brings Planck in line with clustering measurements in *w*KCDM. This behaviour is expected and is consistent with existing analyses (e.g. Di Valentino, Melchiorri & Silk (2021) demonstrated how varying A_{lens} allows Planck to be more consistent with flatness and brings it to a better agreement with the BAO measurements for cosmological models with varying curvature, w, and neutrino mass sum). Here we additionally note that the inclusion of A_{lens} does significantly degrade Planck's ability to constrain σ_{12}.

3.4 Massive neutrinos – *wν*CDM

Finally, we vary the neutrino mass sum, $\sum m_\nu$: here, once again, we supplement our clustering and CMB data sets with Pantheon SNe. As $\sum m_\nu$ exhibits a degeneracy with the dark energy equation of state (for a more detailed discussion, see Hannestad 2005), varying w is expected to degrade the resulting constraints. The addition of SNe Ia, therefore, allows to improve the precision of our constraint through providing a measurement of w.

While clustering alone does not provide a tight upper limit for the neutrino mass ($\sum m_\nu < 1.34$ eV from BOSS + eBOSS at 95 per cent confidence), its combination with Planck does allow for some improvement as compared with Planck alone ($\sum m_\nu < 0.300$ eV for joint constraints versus $\sum m_\nu < 0.321$ eV for Planck). It might, nevertheless, initially seem surprising that the improvement is rather minimal (especially, compared to the constraints obtained from combined Planck full shape clustering analyses in ΛCDM, such as Ivanov, Simonović & Zaldarriaga 2020a; Tanseri et al. 2022). This result can be understood by noting that, due to the degeneracy between the physical matter density, ω_m, and $\sum m_\nu$, a precise measurement of ω_m is required to shrink the upper limit on $\sum m_\nu$. While clustering constraints on either of these parameters are much looser than those of Planck, it may, none the less, be able to improve on Planck's measurement of ω_m by excluding some of the cosmologies in $\omega_m - \omega_{DE}$ space allowed by Planck. This effect happens to be more significant in a ΛCDM cosmology, where the full shape BOSS + eBOSS analysis yields a lower mean value of ω_m, as compared to Planck, resulting in a lower ω_m from a combined measurement and, therefore, reducing the maximum limit of $\sum m_\nu$. As shown in Fig. 6, in the cosmology with varying w the BOSS + eBOSS contour is perpendicular to Planck in $\omega_m - \omega_{DE}$,

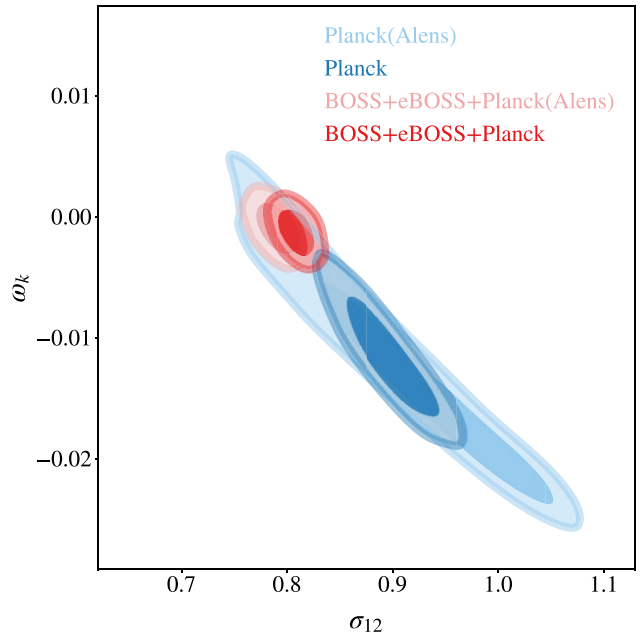

Figure 5. Marginalised posterior contours for σ_{12} and ω_K from Planck and its combination with BOSS + eBOSS in wKCDM. We compare two cases – one with varying $A_{\rm lens}$ (light blue and pink) and a fiducial one, with $A_{\rm lens}$ fixed to 1 (dark blue and red).

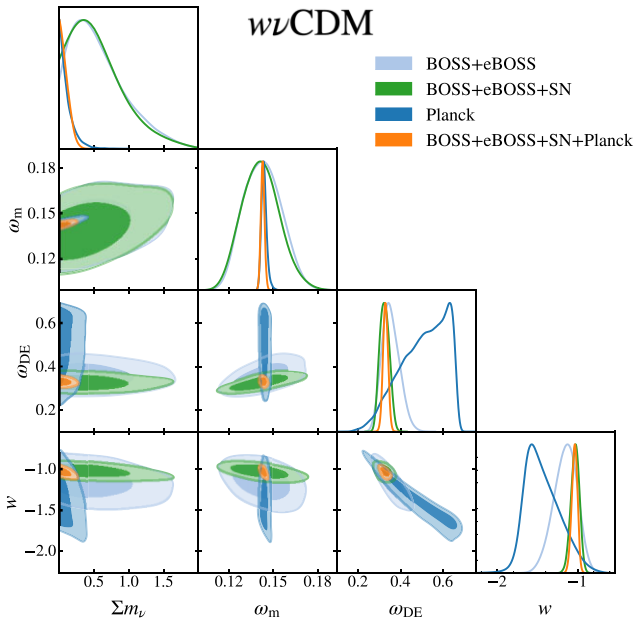

Figure 6. Marginalized posterior contours for dark energy parameters and the neutrino mass sum $\sum m_\nu$ in $w\nu$CDM. Here, we explore varying w together with $\sum m_\nu$. We show constraints from the full-shape clustering analysis of BOSS DR12 galaxies in combination with eBOSS QSOs (light blue), their combination with Pantheon SN Ia measurements (green), CMB constraints by Planck (in dark blue), and the combination of all four data sets (in orange).

resulting in minimal effect on the constraint on ω_m and, consequently, little improvement on the upper mass limit for $\sum m_\nu$.

Our tightest constraint then arises from the combination of BOSS + eBOSS + Planck + SN, which places the upper limit of $\sum m_\nu < 0.211$ eV at 95 per cent confidence. This improvement is due to the fact that the SN constraint on ω_{DE} does result in a tighter constraint on ω_m, which, in turn, shrinks the ω_m, and $\sum m_\nu$ degeneracy.

The SDSS consensus analysis (Alam et al. 2021) provides a lower neutrino mass sum limit for wνCDM of $\sum m_\nu < 0.139$ eV (Planck + BAO + RSD + SN + DES, 95 per cent upper limit); nevertheless, these constraints do include additional data (reconstructed BAO and RSD measurements from full SDSS data as well as measurements from the Dark Energy Survey, DES) and are, therefore, not directly comparable. As described above, the final limit is extremely sensitive to ω_m and, therefore, not only the statistical power of a particular combination of measurements but also the position and orientation of the contours (which may differ for full shape and BAO-only analyses). Here, we only vary neutrino mass and, while there are additional non-standard neutrino properties that could be explored, given our limited constraining power in varying dark energy cosmologies, it is unlikely we might be able to obtain meaningful constraints. It has additionally been shown that in the cosmological constant scenarios, full shape analysis of BOSS and eBOSS galaxy clustering recovers no deviations from standard neutrino properties (Kumar, Nunes & Yadav 2022).

4 CONCLUSIONS

In this work, we performed a full shape analysis of the anisotropic two-point clustering measurements from BOSS galaxy and eBOSS QSO samples together with Planck CMB and Pantheon SN Ia measurements and explored extensions to the ΛCDM cosmological model. In particular, we were interested in models with free dark energy equation of state parameter w and the resulting constraints in physical parameter space.

We demonstrated that CMB recovers a tight degeneracy in the $w-\omega_{DE}$ parameter space and is able to constrain the linear density field variance, σ_{12}, as well as the physical curvature density ω_K, to high precision. The apparent lack of constraining power when using σ_8 is, therefore, only an artefact of using h^{-1}Mpc units when defining the scale on which the density field variance is measured. This approach results in averaging over the posterior of h that Planck does not constrain in evolving dark energy models. We subsequently presented the first CMB measurements of the clustering amplitude today in cosmologies with varying w and found that the clustering amplitude tends to increase for such models. This behaviour is because a more negative w requires a lower initial ω_{DE} value to reach the same constraint at redshift zero. This observation also rules out the evolving dark energy models considered here as a potential way to bring Planck's predicted amount of structure growth closer to weak lensing observations on their own, as such extensions do not affect the initial amplitude of matter fluctuations and the clustering amplitude today σ_{12} is set by the $w - \omega_{DE}$ degeneracy and is well measured even in the extended models.

When, in addition to w, the curvature is also allowed to vary, BOSS + eBOSS and Planck become discrepant, most significantly in the $w - \omega_{DE}$ plane and, subsequently, in the resulting values of σ_{12}, with Planck preferring a 2.4σ higher value than BOSS + eBOSS. Varying dark energy models are, therefore, not able to bring the two probes in a better agreement for curved cosmologies. In addition to this result, our physical curvature density constraint for Planck $\omega_K = -0.0116^{+0.0029}_{-0.0036}$ prefers a curved Universe at 4σ significance, which is 2.4σ higher than what is found using Ω_K.

It is encouraging that the extended model constraints that we derive from our full shape analysis are compatible with a ΛCDM cosmology (with the greatest deviation seen for ω_K but still within $\omega_K = 0$ at 95 per cent confidence) as well as with previous clustering analyses.

We derive the 95 per cent upper limit for the neutrino mass sum of $\sum m_\nu < 0.211$ eV (BOSS + eBOSS + Planck + SN), which is a higher value than that of the SDSS consensus analysis (though the two constraints are not directly comparable, as the consensus analysis makes use of a more extensive data set). When w is varied freely, clustering alone only allows for a modest improvement in the upper limit of $\sum m_\nu$.

Our analysis demonstrates the strength of the physical parameter space in constraining extended cosmologies. While we are currently still unable to place tight constraints on the dark energy parameters directly, we were able to show how even the high-redshift observations place limits on the allowed behaviours. We were also able to provide a consistent picture of the current state of full-shape clustering constraints, which were shown to be highly complementary to the CMB measurements. With CMB providing information on physical matter and curvature densities, as well as setting a strict limit on the allowed clustering amplitude values and clustering offering a way to measure dark energy, we may hope that the Stage-IV surveys will be able to confidently exclude large regions of the extended parameter space.

ACKNOWLEDGEMENTS

We would like to thank Daniel Farrow, and Martha Lippich for their help and useful suggestions. The plots in this paper were produced using GetDist package (Lewis 2019). This research was supported by the Excellence Cluster ORIGINS, which is funded by the Deutsche Forschungsgemeinschaft (DFG; German Research Foundation) under Germany's Excellence Strategy – EXC-2094-390783311.

AE is supported at the AIfA by an Argelander Fellowship.

JH has received funding from the European Union's Horizon 2020 research and innovation program under the Marie Skłodowska-Curie grant agreement no. 101025187.

GR acknowledges support from the National Research Foundation of Korea (NRF) through grant no. 2020R1A2C1005655 funded by the Korean Ministry of Education, Science and Technology (MoEST), and from the faculty research fund of Sejong University in 2022/2023.

Funding for the Sloan Digital Sky Survey IV has been provided by the Alfred P. Sloan Foundation, the U.S. Department of Energy Office of Science, and the Participating Institutions. SDSS-IV acknowledges support and resources from the Center for High-Performance Computing at the University of Utah. The SDSS web site is www.sdss.org.

DATA AVAILABILITY

The clustering measurements from BOSS and eBOSS used in this analysis are publicly available via the SDSS Science Archive Server (https://sas.sdss.org/).

REFERENCES

Abbott T. M. C. et al., 2018, Phys. Rev. D, 98, 043526
Abbott T. M. C. et al., 2019, Phys. Rev. D, 99, 123505
Abbott T. M. C. et al., 2022, Phys. Rev. D, 105, 023520
Ahumada R. et al., 2020, ApJS, 249, 3
Alam S. et al., 2015, ApJS, 219, 12
Alam S. et al., 2017, MNRAS, 470, 2617
Alam S. et al., 2021, Phys. Rev. D, 103, 083533
Alcock C., Paczyński B., 1979, Nature, 281, 358
Anderson L. et al., 2012, MNRAS, 427, 3435
Baumann D., Nicolis A., Senatore L., Zaldarriaga M., 2012, J. Cosmol. Astropart. Phys., 2012, 051
Bel J., Larena J., Maartens R., Marinoni C., Perenon L., 2022, J. Cosmol. Astropart. Phys., 2022, 076
Bel J., Pezzotta A., Carbone C., Sefusatti E., Guzzo L., 2019, A&A, 622, A109
Birrer S. et al., 2020, A&A, 643, A165
Brieden S., Gil-Marín H., Verde L., 2021, J. Cosmol. Astropart. Phys., 2021, 054
Brieden S., Gil-Marín H., Verde L., 2022, J. Cosmol. Astropart. Phys., 2022, 024
Campbell H. et al., 2013, ApJ, 763, 88
Carrilho P., Moretti C., Pourtsidou A., 2023, J. Cosmol. Astropart. Phys., 2023, 028
Catelan P., Lucchin F., Matarrese S., Porciani C., 1998, MNRAS, 297, 692
Catelan P., Porciani C., Kamionkowski M., 2000, MNRAS, 318, L39
Chan K. C., Scoccimarro R., Sheth R. K., 2012, Phys. Rev. D, 85, 083509
Chen S.-F., Vlah Z., White M., 2022, J. Cosmol. Astropart. Phys., 2022, 2, 008
Chevallier M., Polarski D., 2001, Int. J. Mod. Phys. D, 10, 213
Chudaykin A., Dolgikh K., Ivanov M. M., 2021a, Phys. Rev. D, 103, 023507
Chudaykin A., Dolgikh K., Ivanov M. M., 2021b, Phys. Rev. D, 103, 023507
Cole S. et al., 2005, MNRAS, 362, 505
Colgáin E. Ó., Sheikh-Jabbari M. M., 2021, Class. Quant. Grav., 38, 177001
d'Amico G., Gleyzes J., Kokron N., Markovic K., Senatore L., Zhang P., Beutler F., Gil-Marín H., 2020, J. Cosm. Astropart. Phys., 2020, 005
Dawson K. S. et al., 2013, AJ, 145, 10
Dawson K. S. et al., 2016, AJ, 151, 44
DES Collaboration, 2022, preprint (arXiv:2207.05766)
DESI Collaboration, 2016, preprint (arXiv:1611.00036)
Di Valentino E., Melchiorri A., Silk J., 2020, Nat. Astron., 4, 196
Di Valentino E., Melchiorri A., Silk J., 2021, ApJ, 908, L9
Eggemeier A., Scoccimarro R., Smith R. E., 2019, Phys. Rev. D, 99, 123514
Eggemeier A., Scoccimarro R., Smith R. E., Crocce M., Pezzotta A., Sánchez A. G., 2021, Phys. Rev. D, 103, 123550
Eisenstein D. J. et al., 2005, ApJ, 633, 560
Fry J. N., 1996, ApJ, 461
Glanville A., Howlett C., Davis T. M., 2022, MNRAS, 517, 3087
Hagstotz S., Reischke R., Lilow R., 2022, MNRAS, 511, 662
Handley W., 2021, Phys. Rev. D, 103, L041301
Hannestad S., 2005, Phys. Rev. Lett., 95, 221301
Hartlap J., Simon P., Schneider P., 2007, A&A, 464, 399
Heymans C. et al., 2021, A&A, 646, A140
Hinshaw G. et al., 2013, ApJS, 208, 19
Hou J. et al., 2018, MNRAS, 480, 2521
Hou J. et al., 2021, MNRAS, 500, 1201
Ivanov M. M., Simonović M., Zaldarriaga M., 2020a, Phys. Rev. D, 101, 083504
Ivanov M. M., Simonović M., Zaldarriaga M., 2020b, J. Cosmol. Astropart. Phys., 2020, 042
Ivezić Ž. et al., 2019, ApJ, 873, 111
Kaiser N., 1987, MNRAS, 227, 1
Kaufman G. M., 1967, A&A
Kazin E. A., Sánchez A. G., Blanton M. R., 2012, MNRAS, 419, 3223
Kitaura F.-S. et al., 2016, MNRAS, 456, 4156
Kitching T. D. et al., 2014, MNRAS, 442, 1326
Kourkchi E. et al., 2020, ApJ, 902, 145
Kumar S., Nunes R. C., Yadav P., 2022, J. Cosmol. Astropart. Phys., 2022, 060
Laureijs R. et al., 2011, preprint (arXiv:1110.3193)
Lewis A., 2019, preprint (arXiv:1910.13970)
Lewis A., Bridle S., 2002, Phys. Rev. D, 66, 103511
Lewis A., Challinor A., Lasenby A., 2000, ApJ, 538, 473
Linder E. V., 2003, Phys. Rev. Lett., 90, 091301
Lyke B. W. et al., 2020, ApJS, 250, 8
Nishimichi T., Bernardeau F., Taruya A., 2016, Phys. Lett. B, 762, 247
Nishimichi T., Bernardeau F., Taruya A., 2017, Phys. Rev. D, 96, 123515

Otten E. W., Weinheimer C., 2008, Rep. Prog. Phys., 71, 086201
Parkinson D. et al., 2012, Phys. Rev. D, 86, 103518
Percival W. J. et al., 2002, MNRAS, 337, 1068
Percival W. J. et al., 2014, MNRAS, 439, 2531
Perlmutter S. et al., 1999, ApJ, 517, 565
Pezzotta A., Crocce M., Eggemeier A., Sánchez A. G., Scoccimarro R., 2021, Phys. Rev. D, 104, 043531
Planck CollaborationVI, 2020, A&A, 641, A6
Planck CollaborationXIII, 2016, A&A, 594, A13
Reid B. et al., 2016, MNRAS, 455, 1553
Reid M. J., Braatz J. A., Condon J. J., Lo K. Y., Kuo C. Y., Impellizzeri C. M. V., Henkel C., 2013, ApJ, 767, 154
Riess A. G. et al., 1998, AJ, 116, 1009
Riess A. G. et al. 2022, ApJL, 934, L7
Ross A. J. et al., 2020, MNRAS, 498, 2354
Sánchez A. G. et al., 2012, MNRAS, 425, 415
Sánchez A. G. et al., 2017, MNRAS, 464, 1640
Sánchez A. G., 2020, Phys. Rev. D, 102, 123511
Sánchez A. G., Baugh C. M., Percival W. J., Peacock J. A., Padilla N. D., Cole S., Frenk C. S., Norberg P., 2006, MNRAS, 366, 189
Sánchez A. G., Ruiz A. N., Jara J. G., Padilla N. D., 2022, MNRAS, 514, 5673
Scoccimarro R., 2004, Phys. Rev. D, 70, 083007
Scolnic D. M. et al., 2018, ApJ, 859, 101
Semenaite A. et al., 2022, MNRAS, 512, 5657
Sheth R. K., Chan K. C., Scoccimarro R., 2013, Phys. Rev. D, 87, 083002
Simon T., Zhang P., Poulin V., Smith T. L., 2022, preprint (arXiv:2208.05929)
Spergel D. N. et al., 2003, ApJS, 148, 175
Tanseri I., Hagstotz S., Vagnozzi S., Giusarma E., Freese K., 2022, J. High Energy Astrophys., 36, 1
Taruya A., Bernardeau F., Nishimichi T., Codis S., 2012, Phys. Rev. D, 86, 103528
Taruya A., Nishimichi T., Saito S., 2010, Phys. Rev. D, 82, 063522
Tegmark M. et al., 2004, ApJ, 606, 702
Tröster T. et al., 2020, A&A, 633, L10
Tröster T. et al., 2021, A&A, 649, A88
Vagnozzi S., Di Valentino E., Gariazzo S., Melchiorri A., Mena O., Silk J., 2021, Phys. Dark Univ., 33, 100851
Zarrouk P. et al., 2018, MNRAS, 477, 1639
Zhao C. et al., 2021, MNRAS, 503, 1149

APPENDIX: ADDITIONAL CONSTRAINTS

In this section, we present the constraints on parameters omitted in Table 2, including constraints in the 'traditional' parameter space (Table A1). The physical parameters (i.e. not defined through h units) constrained by our data include the physical matter density $\omega_{\rm m}$, the spectral index $n_{\rm s}$ and the (log) amplitude of initial density fluctuations $\ln 10^{10} A_{\rm s}$. For completeness, we include the traditional parameters σ_8 (linear density field variance as measured on the scale of $8h^{-1}$Mpc whose physical equivalent is σ_{12}), Hubble parameter H_0 and the relative densities of matter ($\Omega_{\rm m}$), dark energy ($\Omega_{\rm DE}$), and curvature ($\Omega_{\rm K}$).

In general, we expect that the constraints on these parameters are degraded in comparison to their physical equivalents due to averaging over the posterior of H_0, which tends to be less well constrained in these extended cosmologies (this is most evident when comparing σ_{12} with σ_8).

Table A1. Marginalized posterior constraints (mean values with 68 per cent confidence interval, for $\sum m_\nu$ – 95 per cent confidence interval) derived from Planck CMB and the full shape analysis of BOSS + eBOSS clustering measurements on their own, as well as in combination with each other and with Pantheon SN Ia measurements. All of the models considered here vary dark energy equation of state parameter w, w_aCDM additionally allows a redshift evolution for w, w*K*CDM varies curvature and $w\nu$CDM varies neutrino mass sum $\sum m_\nu$. Note that for w*K*CDM the joint BOSS + eBOSS + Planck constraints should be interpreted bearing in mind that BOSS + eBOSS and Planck are discrepant in this parameter space.

		BOSS + eBOSS	BOSS + eBOSS + Planck	BOSS + eBOSS + Planck + SN
wCDM	σ_8	0.798 ± 0.047	0.828 ± 0.017	0.818 ± 0.012
	H_0	$69.8^{+3.1}_{-3.6}$	$69.6^{+1.4}_{-1.6}$	68.62 ± 0.84
	$\Omega_{\rm m}$	$0.280^{+0.017}_{-0.021}$	0.295 ± 0.013	0.3026 ± 0.0080
	Ω_Λ	$0.720^{+0.021}_{-0.017}$	0.705 ± 0.013	0.6974 ± 0.0080
	$\omega_{\rm m}$	$0.137^{+0.011}_{-0.013}$	0.1426 ± 0.0011	0.1424 ± 0.0011
	$n_{\rm s}$	0.990 ± 0.055	0.9661 ± 0.0042	0.9665 ± 0.0041
	$\ln 10^{10} {\rm A_s}$	3.02 ± 0.21	3.043 ± 0.016	3.044 ± 0.016
w_aCDM	σ_8	0.793 ± 0.045	$0.818^{+0.019}_{-0.022}$	0.822 ± 0.012
	H_0	$70.1^{+3.7}_{-4.4}$	$68.1^{+2.0}_{-2.8}$	68.72 ± 0.86
	$\Omega_{\rm m}$	$0.281^{+0.026}_{-0.030}$	$0.309^{+0.024}_{-0.021}$	0.3025 ± 0.0081
	Ω_Λ	$0.719^{+0.030}_{-0.026}$	$0.691^{+0.021}_{-0.024}$	0.6975 ± 0.0081
	$\omega_{\rm m}$	0.138 ± 0.012	0.1428 ± 0.0012	0.1427 ± 0.0011
	$n_{\rm s}$	0.983 ± 0.054	0.9656 ± 0.0042	0.9658 ± 0.0041
	$\ln 10^{10} {\rm A_s}$	3.00 ± 0.20	3.042 ± 0.016	3.042 ± 0.016
w*K*CDM	σ_8	0.770 ± 0.049	0.834 ± 0.019	0.819 ± 0.012
	H_0	$68.9^{+2.9}_{-3.4}$	$69.7^{+1.4}_{-1.6}$	68.46 ± 0.91
	$\Omega_{\rm m}$	0.292 ± 0.019	0.292 ± 0.014	$0.3032^{+0.0077}_{-0.0086}$
	Ω_Λ	0.829 ± 0.073	0.710 ± 0.015	$0.6982^{+0.0085}_{-0.0076}$
	$\Omega_{\rm K}$	-0.121 ± 0.078	-0.0025 ± 0.0026	-0.0014 ± 0.0024
	$\omega_{\rm m}$	$0.139^{+0.011}_{-0.013}$	0.1419 ± 0.0013	0.1420 ± 0.0013
	$n_{\rm s}$	$0.975^{+0.060}_{-0.053}$	0.9679 ± 0.0046	0.9676 ± 0.0045
	$\ln 10^{10} {\rm A_s}$	2.80 ± 0.26	3.041 ± 0.016	3.043 ± 0.016
$w\nu$CDM	σ_8	$0.795^{+0.041}_{-0.048}$	0.822 ± 0.018	$0.816^{+0.016}_{-0.013}$
	H_0	70.3 ± 3.5	$70.0^{+1.5}_{-1.8}$	68.66 ± 0.85
	$\Omega_{\rm m}$	$0.288^{+0.019}_{-0.022}$	0.293 ± 0.013	0.3028 ± 0.0083
	Ω_Λ	$0.712^{+0.022}_{-0.019}$	0.707 ± 0.013	0.6972 ± 0.0083
	$\omega_{\rm m}$	$0.143^{+0.012}_{-0.014}$	$0.1433^{+0.0013}_{-0.0016}$	0.1427 ± 0.0013
	$n_{\rm s}$	$1.066^{+0.070}_{-0.11}$	0.9659 ± 0.0039	0.9665 ± 0.0041
	$\ln 10^{10} {\rm A_s}$	$3.18^{+0.23}_{-0.26}$	3.043 ± 0.016	3.045 ± 0.016

This paper has been typeset from a TEX/LATEX file prepared by the author.